RSC Advances

ROYAL SOCIETY OF CHEMISTRY

www.rsc.org/advances

A Novel Photomineralization of POME over UV-Responsive TiO_2 Photocatalyst: Kinetics of POME Degradation and Gaseous Product Formations

Kim Hoong Ng[1], *Chin Kui Cheng*[1,2,3*]

[1] Faculty of Chemical & Natural Resources Engineering,

[2] Centre of Excellence for Advanced Research in Fluid Flow,

[3] Rare Earth Research Centre,

Universiti Malaysia Pahang, Lebuhraya Tun Razak, 26300 Gambang Kuantan, Pahang, Malaysia

*Corresponding Author. Tel: +60-9-5492896, Fax: +60-9-5492889

E-mail: chinkui@ump.edu.my

Abstract

Traditionally, palm oil mill effluent (POME) is treated via open ponding system, which however is land-intensive and requires long hydraulic retention time. For the first time, this paper reports, simultaneously, the kinetics of photocatalytic degradation of POME and the assessment of its gaseous product formations. Characterization of the as-received UV-responsive TiO_2 showed that anatase was the predominant crystalline phase with an estimated crystallite size of 45.7 nm and band gap energy of 3.15 eV based on the UV-Vis DRS scanning. Moreover, N_2-physisorption revealed that the BET specific surface area for TiO_2 was 8.73 m^2 g^{-1} with pore size of 22.4 nm. When the photoreactor was blanketed with N_2 gas only at a TiO_2 loading of 0.5 g/L, POME degradation was only 4%. Significantly, in the presence of O_2, the degradation of POME achieved 23%, and can even attain a maximum of 52.0% at TiO_2 loading of 1.0 g/L after 240 min of UV-irradiation. This has demonstrated that the hydroxyl generation rate from water species (prevalent in

N_2-blanket) was considerably slower compared to the hydroxyl generation from the superoxide pathway that originates from externally-supplied O_2. It was also found that the POME degradation kinetics adhered to the 1st-order reaction with specific reaction rates (*k*) ranging from 0.70×10^{-3} to 2.90×10^{-3} min^{-1}. Interestingly, our assessment of the gaseous product formations revealed that the photoreaction employing 1.0 g/L TiO_2 produced the highest amount of CO_2 (38913 μmol) while 0.5 g/L TiO_2 produced the highest amount of CH_4 (361 μmol). From the FTIR scanning of used catalyst, we can confirm that the chemisorption of organics was practically absent. This has led us to believe that the primary role of TiO_2 was to generate hydroxyls for direct attack on the organic compounds in the POME and eventually decompose them into simpler intermediates, CH_4, CO_2, and water. Moreover, after 20 h under the UV irradiation, POME degradation attained 78.0% and the final COD level dropped to 37 ppm, which is safe to be discharged.

Keywords: POME; Photocatalysis; Photomineralization; Titania

1. Introduction

Malaysia and Indonesia collectively own large swaths of arable land for oil palm plantation. This has propelled both countries to become top producers of palm oil commodity. In 2014 alone, 62.34 million of palm oil was traded globally, with 20 million tons of them from Malaysia. Indeed, the global annual consumption of palm oil is expected to increase to 78 million by the year 2020 due to the world population growth[1]. Consequently, it is anticipated that the effluent from palm oil mills will spike. Past research report[2] indicates that 0.5 – 0.75 tons of POME is generated for every tonnage of fresh fruit bunch processed. Significantly, raw POME is acidic (pH 4.5 – 5), hot (353 – 363 K) and thick brownish colloidal wastewater containing 95 – 96% of

water, 4 – 5% of total solids including 2 – 4% of suspended solids, as well as 0.6-0.7% of oil and grease [3]. Besides, it also contains organic matters such as lignin (4700 ppm), phenolics (5800 ppm), pectin (3400 ppm) and amino acids [4-6]. Consequently, POME can inflict serious environmental problem if discharged untreated owing to its high chemical oxygen demand (40,000 to 100,000 ppm) and biochemical oxygen demand (25,000 to 65,000 ppm) [7-9].

The conventional treatment adopted in Malaysia is an open ponding system which is comprised of three stages, viz. anaerobic, facultative and algae process. Finally, it passes through a settling pond for sedimentation process. Overall, 90 days of hydraulic retention time (HTR) is required for this treatment [10]. Consequently, massive land area is required for creating the lagoon to hold the POME. Unfortunately, more often than not, the POME discharge from the final pond (settling pond) fails to meet the discharge standard in Malaysia [11]. In 1977, Malaysia's Department of Environmental has made it a mandatory for palm oil millers to reduce the POME's BOD standard from the initial values of 25,000 to 65,000 ppm BOD level, to 100 ppm threshold. Significantly, in recent years, this BOD level has been further revised down to 20 ppm[12]. Although there is no specific discharge limit for COD under the existing regulatory framework, the Malaysia Sewage and Industrial Effluent Discharge Standard set the COD limit for industrial wastewater to 50 ppm level.

Indeed, many innovative methods to increase the efficiency of POME treatment have been reported, for instance, 95.1-98.7% of COD removal was achieved by Chan and co-workers[13] through anaerobic digestion. In addition, Ahmad et al.[14] reported a 98.4% of COD removal through membrane technology. Moreover, the efficiency of membrane technology can be further enhanced to 99.1% of COD removal when combined with biological method [15]. All these proposed methods have delivered

promising results; however, their cost and operation procedures are neither cheap nor easy to control.

Significantly, there are voluminous publications on the subject of advanced oxidation process (AOP) for the destruction of organic compound. In the AOP technique, photocatalytic degradation can be employed effectively to degrade petroleum refinery wastewater. More than 78% of COD reduction was achieved after 120 min of UV irradiation over nano-TiO_2 photocatalyst [16]. On the other hand, Vilar and co-workers[17] studied the treatment of textile wastewater by solar-driven advanced oxidation process that has led to 98% of decolourization and 89% of mineralization after 7.2 kJ_{UV} L^{-1} and 49.1 kJ_{UV} L^{-1}. Coincidentally, Lima and coworkers[18] have also reported on 98% of color removal in textile wastewater after 30 min of solar irradiation using polypyrrole as photocatalyst. Similar to the aforementioned wastewaters, POME also has substantial amount of organic compound judging by its high level of COD and BOD[12]. Moreover, 'green energy' can be generated through the photo-mineralization of organics, for instance, photocatalysis of methanol solution into H_2 over p-type NiO-based catalyst[19]. Besides, H_2 has also been successfully generated from glycerol over the Pt/TiO_2 photocatalysis under solar irradiation [20]. With the same photocatalyst, Languer and co-workers[21] have generated H_2 from methanol, ethanol, glycerol and phenol solutions at room temperature. Significantly, to our best knowledge, no prior works have been reported for renewable energy source production as a form of energy extraction from POME via photocatalytic degradation. Indeed, taking our inspiration from the previous AOP works, we have mooted the idea of adopting photocatalytic pathway as a new technique to degrade POME with our primary focus was only on reducing the COD level[22-23]. TiO_2-based photocatalysts were employed throughout our earlier works, as this type of

photocatalyst is the most effective material for UV-activated photoreaction. In fact, TiO_2 is still the preferred photocatalyst for the current study, primarily due to its low toxicity, high resistance towards corrosion and also it is a readily-available semiconductor[24]. Indeed, according to Fujishima et al.[25], TiO_2 is an excellent photocatalyst material for environmental purification. Besides, the photo-degradability of organic substrates over TiO_2 has been presented in numerous past researches, i.e. Wang and co-workers[26] reported on 80% of o-cresol oxidized after 400 min of UV irradiation over Pt/TiO_2 photocatalysis while Barka et al.[27] have reported complete degradation of phenol over TiO_2 photocatalysis after 120 min of UV irradiation. On the other hand, with similar conditions, 40% of phenol degradation after 60 min of UV exposure was recorded by Choquette-Labbé et al.[28]. Although the use of pristine TiO_2 photocatalyst to treat organic waste may not be novel, its application in photocatalytic degradation of POME is sufficiently novel. Significantly, it represents one of the larger programs in our laboratory to examine the photocatalytic technique to degrade POME, whilst simultaneously assessing its gas products to evaluate its potential in producing renewable energy such as methane (CH_4). Therefore, the primary objective for the current study is to apply AOP technique to treat the POME to the allowable discharge COD level (maximum 50 ppm) over the titania (TiO_2) photocatalyst, while at the same time analysing its gaseous products that results from the photomineralization.

2. Methodology

2.1 POME Sampling and Preservation

The POME for current study was directly collected from the settling pond of a local palm oil mill located in the province of Kuantan, Malaysia. The POME was stored in a black, air-tight container to avoid the light exposure during the

transportation. Besides, the container was filled up to the brim to avoid reaeration. Immediately, the sample was filtered to remove the suspended solids followed by storing at 277 K for preservation. Besides, the initial BOD, COD and pH values of POME sample were tested right after the pre-treatment procedure. For BOD, dilution water was prepared by mixing 1 mL of phosphate buffer, magnesium sulfate, calcium chloride, ferric chloride solution and diluted to 1000 mL by distilled water. Then, 10 mL of POME sample was diluted with 300 mL by using dilution water. pH of the diluted POME was adjusted to the range of 6.5 to 7.5 before transferring into the incubation bottle. The dissolved oxygen (DO) concentration for POME sample was analyzed by using dissolved oxygen meter before sealing the incubation bottle. Lastly, the incubation bottle was placed in the BOD incubator (Temperature = 298 K) for five days before the final DO value was taken. BOD level can be calculated according to the Equation (1).

$$\text{BOD (ppm)} = (D_1 - D_2) / P \quad (1)$$

where D_1 and D_2 are the initial and final DO values of POME sample, and P denotes for the decimal volumetric fraction of sample used.

For COD analysis, 2 ml of POME sample was injected into the COD vial and pre-heated to 473 K for 2 h before being measured using Hach DRB-200 COD instrument. The pH of the POME sample for the photocatalytic degradation studies was analysed using litmus paper.

2.2 Characterization of TiO_2 Photocatalyst

The photocatalyst for current study was a commercial TiO_2 which was directly sourced from Sigma-Aldrich. The crystalline phase and its size were identified via X-ray diffraction (XRD). The XRD pattern was obtained from the Philips X'Pert instrument using X-ray source from CuKα (λ=1.542 Å) at 30 kV and 15 mA. From

the XRD diffractogram, the crystallite size was computed using the Scherrer equation as shown in (2):

$$D = \frac{k_{sch}\lambda}{\beta_d \times \cos\theta} \quad (2)$$

where D is the crystallite size in nm, λ is wavelength of X-ray (nm), β_d is the angular width at half maximum intensity (radian), θ is the Bragg's angle degree and k_{Sch} is the Scherrer constant and equals to 0.93 [29].

The morphology structure and the particle size of the catalyst were determined through FESEM analysis employing JEOL FESEM JSM-7100F with a magnification of 100 k*X*. In addition, the specific surface area of the photocatalyst was analysed from N_2 physisorption technique using the Thermo-Scientific Surfer unit. The temperature of N_2 used was 77 K with cross-sectional area of 16.2 $Å^2$. The specific surface area of TiO_2 can be estimated using the following equation:

$$S_{BET} = \frac{v_m \times N \times s}{V \times g} \quad (3)$$

where v_m is the volume of gas adsorbed corresponding to monolayer coverage, N is the Avogadro's constant, s denotes for cross-sectional area of N_2, V represents molar volume of N_2 and lastly g is the mass of TiO_2 used in analysis.

Furthermore, the optical property of the photocatalyst was determined from the UV-vis diffuse reflectance spectroscopy measurements provided by a Jasco V-550 spectrophotometer equipped with an integrating sphere, for band-gap energy (E_{bg}) determination. The wavelength of absorption spectrum measurement was ranging from 190 to 900 nm. The light source used was a deuterium lamp for wavelength ranging from 190 to 350 nm (UV region) and a halogen (WI) lamp for 340 to 2500 nm (VIS/NIR region). The original coordinates of the spectra (reflectance vs.

wavelength) were transformed to Kubelka–Munk function (*K*) vs. photon energy (*h*ν). The final plot of $(ahv)^{½}$ as a function of *h*ν is in accordance with the theoretical equation (4):

$$ahv = const(h\nu - E_{bg})^2 \quad (4)$$

whereby "*a*" is an absorption coefficient of the photocatalyst and E_{bg} is the band gap energy. The Kubelka–Munk function (*K)* calculated from the reflectance spectra is pre-determined to be directly proportional to the absorption coefficient (α)). The current work employed method based on the fitting of the experimental dependences by Boltzmann symmetrical function using non–linear regression. Finally, Fourier transform infrared spectroscopy (FTIR) analysis was conducted on the fresh and spent TiO_2 by using a Perkin Elmer Spectrum 100 instrument to examine the presence of functional groups on TiO_2 surface. The range of wavenumber employed for the analysis was 4000 to 1000 cm^{-1}. For the spent catalyst (collected from the filtration of POME slurry, post longevity reaction), it was gently draped with smooth and clean tissue for drying purpose, followed immediately by analysis using attenuated total reflectance (ATR)-FTIR.

2.3 Photocatalytic degradation of POME

The photocatalytic degradation of POME under the UV light was carried out in an air-tight photoreactor system. The whole photoreactor system was meticulously-covered with aluminum foil to minimize energy loss, and stored under dark environment to prevent external stray light from interfering with the experiment. A 500 mL Pyrex quartz reactor was used for the photoreaction of POME. During the reaction, 450 mL of pre-treated POME (COD level controlled in the range of 155 – 170 ppm) was mixed with pre-determined TiO_2 photocatalyst loading, and stirred vigorously for 30 min. At the same time, pure zero-grade O_2 gas was metered into the

reactor to provide O_2 blanket and to establish equilibrium point of dissolved O_2 in the POME wastewater. The cooling water compartment that jackets the UV light source was continuously circulated with water to remove dissipated heat from the UV lamp. This would ensure that the reaction slurry was always maintained at the room temperature. Subsequently, the 100 watt UV lamp, with an intensity averaging 11.0 W/m^2 was switched on, to initiate the photoreaction. For sampling purpose, 5 ml of aliquot was withdrawn from the reactor at every 60 min interval for COD measurement using Hach DRB-200 COD instrument. With these COD results, the degradation, X (%) is calculated by using Equation (5).

$$X(\%) = \left(1 - \frac{C_A}{C_{AO}}\right) \times 100 \quad (5)$$

where C_{AO} is the initial COD value and C_A denotes for the COD value at time, *t*.

During the reaction, the gas sample was collected at time intervals of 30, 60, 120, 180 and 240 min, and subsequently eluted by gas chromatography (GC) with two packed bed columns, viz. Supelco Molecular Sieve 13x (10 ft × 1/8 in OD × 2mm ID, 60/80 mesh, SS) and Agilent HayeSep DB (30 ft × 1/8 in OD × 2 mm ID, 100/120 mesh, SS). The carrier gas used was He gas with the flow rate of 20 ml/min. Oven and detector were operated at 393 and 423 K, respectively.

3 Results and Discussion

3.1 Characterization of TiO_2

Commercial TiO_2 which was procured from Sigma-Aldrich was subjected to the XRD measurement without any pre-treatment and the diffractogram obtained is presented in Figure 1a. Based on Figure 1a, the peaks recorded at 2θ readings of 25.5°, 37.2°, 38.0°, 38.8°, 48.2°, 54.0°, 55.0°, 62.0°, 70.0° and 76.0° have indicated that anatase was indeed the predominant crystalline phase. All the peaks were sharp which

was indicative of good crystallinity of the solid sample. The highest peak was observed at 2θ reading of 25.5°. Based on this highest peak, the crystallite size was estimated as 45.7 nm.

Through FESEM characterization technique (cf. Figure 1b), image of spherical particles of TiO_2 with smooth surface was observed. The non-uniformity of the particle sizes was observed too, judging by the different particle sizes estimated. Based on Figure 1b, the particle size was estimated ranging from 70 – 100 nm.

In addition, Figure 1c shows the isotherm of TiO_2 obtained from N_2 physisorption. It demonstrates that the adsorption and desorption isotherms did not coincide to each other. The possible explanation for this phenomenon is the occurrence of adsorption hysteresis. This obtained isotherm can be classified as a type-V isotherm according to the IUPAC identification system, which indicates the mesoporous structure material (2-50 nm). Indeed, the estimation using Barrett-Joyner-Halenda (BJH) equation gave an average TiO_2 pore diameter of 22.4 nm. Besides, the N_2 physisorption also reveals that the virgin TiO_2 has a considerably low BET specific surface area (8.73 m^2 g^{-1}) by employing Equation (3).

For the optical property characterization, Figure 2a shows the diffuse reflective UV-vis spectrum of TiO_2. The results obtained demonstrated excellent light energy spectrum absorption at $\lambda < 350$ nm (UV region), whilst in the visible light region, the absorption value has plummeted. This observation reaffirms the UV-photosorption ability of TiO_2 material. Subsequently, the band gap energy of TiO_2 photocatalyst was estimated by plotting $(ahv)^{1/2}$ versus band gap energy (hv) (Figure 2b) using Kubelka-Munk functions (cf. Equation (4)). Based on Figure 2b (red dotted line), the band gap energy of TiO_2 was 3.15 eV, which is in accordance with the findings of past works (3.15 ~ 3.27 eV) [30].

3.2 Photocatalytic degradation of POME

3.2.1 Preliminary works

In order to investigate the COD content from the last pond (settling pond) to determine whether it meets the standard discharge limit, two different samplings from the same pond were carried out, analysed and subsequently compared with the *Standard A* wastewater (Malaysia's Environmental Law). POME-1 denotes for the 1st sample that was taken in the February 2015, while POME-2 denotes for sample taken four weeks after the POME-1. Table 1 summarizes the findings.

Based on Table 1, the pH value was well within the prescribed standard. Nonetheless, the BOD and COD for both samples (80 ppm and 170 ppm for POME-1; 126 ppm and 240 ppm for POME-2) were well over the maximum allowable standard set by the existing regulation. This finding is consistent with past research[11], in which the ponding system is unable to degrade POME down to the permitted level for discharge.

Significantly, the variation (comparing POME-1 and POME-2) in COD and BOD values also showed the difficulty in controlling the quality of final discharge from the ponding treatment. For the current study, the COD level of POME was well-controlled within the range of 155 to 170 ppm for standardization purpose, through dilution. A series of photoreactions were conducted employing 0.5 g/L of TiO_2 at room temperature, but at different O_2 flowrates. The choice of 0.5 g/L was in accordance with typical catalyst loading for this kind of study. Figure 3 shows the degradation achieved at t = 240 min for different sets of photoreactions.

For the case of 0 ml/min O_2 flowrate, N_2 gas was purged into the photoreactor for 30 min followed by metering at 30 ml/min to provide N_2-blanket. It can be observed that only 4% of degradation was achieved after 240 min of UV irradiation.

Significantly, an increasing trend was observed from 0 ml/min O_2 flowrate (N_2-blanket) to the highest degradation (circa 23.0%) at O_2 flowrate of 70 ml/min. Beyond that, the degradation efficiency actually decreased with the O_2 flowrate, i.e. at 150 ml/min, the degradation was noticeably lower at 16.0%.

The following outlined mechanisms describe the generation of hydroxyl radicals which can shed some light into the degradation trend (cf. Figure 3). Based on the concept of photocatalytic degradation, upon photo-excitement, a negatively charged electron and positively charged hole are generated (cf. (M1)). The generated hole (h^+) would attack on H_2O, producing a pair of hydroxyl ($OH^\bullet$) and proton (H^+) (refers to (M2)). The hydroxyl radicals are highly reactive and responsible for organic compounds degradation[31]. On the other hand, the generated electron was accepted by O_2 to form super-oxide anions, O_2^- (M3). Subsequently, the O_2^- ion would react with H^+ (from (M2)) through (M4) and (M5). Hydrogen peroxide (H_2O_2) formed would further dissociate into $OH^\bullet$ free radical groups upon exposure to the UV irradiation (M6). These $OH^\bullet$ free radical generation steps are consistent with past researches[32-35].

$$TiO_2 \xleftrightarrow{hv} e^- + h^+ \qquad \text{(M1)}$$

$$h^+ + H_2O \leftrightarrow OH^\bullet + H^+ \qquad \text{(M2)}$$

$$e^- + O_2 \leftrightarrow O_2^- \qquad \text{(M3)}$$

$$O_2^- + H^+ \leftrightarrow HO_2^\bullet \qquad \text{(M4)}$$

$$O_2^- + H^+ + HO_2^\bullet \leftrightarrow H_2O_2 + O_2 \qquad \text{(M5)}$$

$$H_2O_2 \xrightarrow{hv} 2OH^\bullet \qquad \text{(M6)}$$

As aforementioned, when O_2 was practically absent as in the case of N_2-blanket, a meagre POME degradation was recorded (cf. Figure 3) whilst in contrast, a significant increment in degradation was recorded when O_2 was metered into the system. Therefore, it can be surmised that the rate of hydroxyl radical generation via steps

(M3) – (M6) was significantly faster than the steps (M1) to (M2). Moreover, unlike N_2, O_2 is an electron-acceptor that will hold the electron generated upon excitement of TiO_2 photocatalyst, preventing recombination of holes(h^+) and electrons(e^-); eventually this would have enhance the photo-degradability of POME. This likely explained the increase in degradation trend when O_2 flowrate was varied from 0 to 70 ml/min. However, beyond 70 ml/min, formation of large bubbles in the POME liquor may have induced boundary layer effects. Due to this physical limitation, photocatalytic degradation of POME was affected. Therefore, the best O_2 flowrate for POME degradation in the current work was 70 ml/min and hence was employed thereafter for further POME degradation studies.

3.2.2 Blank Runs

In order to be certain that the POME degradation in the current work was primarily due to photocatalytic effect, two blank runs (adsorption study and photolysis) were conducted.

For the adsorption study, the experiment was conducted with 0.5 g/L of TiO_2 and 70 mL/min of O_2 flowrate under dark environment. The results obtained shows that the COD level and eventually the degradation for this set were nearly invariant with time. This suggests that the adsorption process was practically negligible for the current type of photocatalyst. Significantly, this can be ascribed to the considerably low BET specific surface area (8.73 m^2 g^{-1}) which has limited the physisorption of organics onto the photocatalyst's surface. For the photolysis experiment, the run was conducted in the absence of TiO_2 photocatalyst but 70 mL/min of O_2 under UV light irradiation. After 240 min of UV irradiation, no significant degradation to the COD values (< 2.0%) was observed. Significantly, GC analysis of the collected gas samples for both blank runs did not show any traces of biogas (mixture of CO_2 and CH_4). This

only serves to confirm that neither adsorption nor photolysis processes occurred at significant rates to simultaneously degrade POME and yield any gas compounds.

3.2.3 Effects of TiO_2 Loadings

Photoreaction runs were conducted with 70 ml/min of oxygen flowrate and presence of UV-light (100 W) but at different TiO_2 loading to determine the effects of varying photocatalyst loading, and also to identify the best TiO_2 loading. The results obtained are shown in Figure 4a.

In terms of COD level, as aforementioned, the initial COD level was well controlled within the range of 155 ppm to 170 ppm. The lowest COD level was achieved by the photoreaction with 1.0 g/L loading, in which POME was degraded to below 80 ppm from the initial COD of 160 ppm after 240 min of UV irradiation. On the other hand, POME with 0.1 g/L of photoreaction exhibited the highest COD reading after 240 of UV irradiation. However, a noticeable degradation, from 155 ppm to 130 ppm, was still observed despite the high final COD level. Significantly, in terms of degradation, compared to photolysis (< 2.0% degradation), an obvious increment in COD degradation was recorded when TiO_2 was present. The results obtained demonstrated that more than 15.0% of organics in POME was degraded after 240 min of UV irradiation when 0.1 g/L of TiO_2 was employed. Furthermore, the highest POME degradation, 52.0%, was achieved by photoreaction over TiO_2 loading of 1.0 g/L. Generally, higher TiO_2 loading indicates higher organics degradation rate. Thus, an increasing trend of COD degradation rate was obtained from 0.1 to 1.0 g/L. However, beyond 1.0 g/L, the degradation efficiency reduced. This may be ascribed to the increase in TiO_2 loading that would have increased the solution opacity. Eventually, this has induced shielding effects that diminished the penetration of the

light into the solution slurry. Significantly, this confirmed that 0.1 g/L loading of TiO_2 was the best.

By employing the method of initial rates[36] to obtain the initial POME degradation rate $\left(-r_{COD}^{o}\right)$ via finite differentiation of transient COD profiles, Figure 5 was further plotted to show the effects of initial TiO_2 loading on $\left(-r_{COD}^{o}\right)$. It can be seen that the POME degradation rate peaked at TiO_2 loading of 1.0 g/L. Thereafter, the negative effects arising from TiO_2 particle shielding has largely overtaken the beneficial catalytic effects. The data in Figure 5 may be presented by the following empirical formula which fitted well with the experimental data ($R^2 = 0.97$).

$$-r_{COD} = \frac{k_{cat} W_{cat}^{2.6}}{S^{4.6} + W_{cat}^{4.6}} \tag{6}$$

where W_{cat} is TiO_2 loading (g/L), k_{cat} is the pseudo-rate constant for TiO_2 loading (1.0 ppm g^2/ min L^2), and S is the parameter for volumetric light shielding effect (1.052 g/L) with a correlation coefficient of 0.97.

Langmuir-Hinshelwood (LH) rate law model were subsequently employed to model the kinetics data (cf. Figure 4a). For irreversible and surface limited reaction that occurs on single site, the reaction rate can be described by:

$$-r_{COD} = -\frac{dC_A}{dt} = \frac{kC_A}{1 + K_A C_A} \tag{7}$$

where $-r_{COD}$ = COD degradation rate (ppm min^{-1})

The concentration of oxygen remained constant throughout the experiments as O_2 was continuously supplied to the reacting system. Due to the low concentration of organics in the sample, the denominator can further simplified into 1 ($1 >> K_A C_A$). Ultimately, this was a reaction system that displayed first-order reaction kinetics.

$$-\frac{dC_A}{dt} = kC_A \quad (8)$$

By integrating both sides of Equation (8), the following expression was obtained:

$$\ln\frac{C_{AO}}{C_A} = kt \quad (9)$$

where C_{AO} = initial COD level of the sample (ppm)

C_A = COD level of the sample at time *t* (ppm)

k = apparent specific reaction rate (min^{-1})

t = time (min)

Figure 4b shows the resulting modelling exercise. In lieu of excellent linearity, it can be concluded that the decomposition of organics in POME indeed ahered to 1st order reaction.

In addition, the *k*-values can be obtained by determining the slope of each graph in Figure 4b. The *k*-values of the photoreactions are summarized in Table 2. Based on Table 2, *k* values that were sorted according to the highest to lowest ranking were 2.90×10^{-3} min^{-1} (1.0 g/L TiO_2 loading) > (2.60×10^{-3} min^{-1} (1.5 g/L loading) > 2.10×10^{-3} min^{-1} (2.0 g/L loading) > 1.60×10^{-3} min^{-1} (0.7 g/L loading) > 1.10×10^{-3} min^{-1} (0.5 g/L loading) > 0.1 g/L (0.70×10^{-3} min^{-1}). Interestingly, this trend is also consistent with the profiles in Figures 4 and 5.

Error analysis was subsequently carried out to justify the adequacy of the model developed. Figure 6 shows the parity plot that suggests a good agreement with R^2 value of 0.98 between the predicted and actual $\ln(C_{AO}/C_A)$ values[37].

In terms of the assessment of gaseous products that was collected during the POME irradiation by UV-light, Figure 7 shows the transient profiles of gas products

that were produced directly from the photocatalytic degradation of POME. Significantly, two types of gaseous products were formed, viz. CO_2 and CH_4. From Figure 7a, a general trend of CO_2 production can be observed for all sets of experiments, in which the production rate increased at the initial stage of photoreaction and peaked at 60 min. Thereafter, the production rate decreased. The decrease in CO_2 production could be due to the exhausting of organics in the POME sample. This can be confirmed by the recyclability study which is presented in Section 3.2.5. Interestingly, CH_4 was also produced and its production rate (cf. Figure 7b) was comparatively stable over the entire irradiation period. The detection of both CO_2 and CH_4 indicated a continuous carbon loss from the liquid POME (albeit may not be in its entirety) as gaseous products, symptomatic of photomineralization process.

From Figure 7, CO_2 seems to be the major product from the POME photocatalytic degradation. Based on Manickam et al.[38], with continuous supply of O_2 to the system, the organics in POME have higher tendency to be degraded into CO_2 compared to the other species. This is unsurprising considering that CO_2 (ΔG_f^o = -394.39 kJ/mol) is thermodynamically very stable species [39], and therefore very easy to form. For CH_4 species (a component in natural gas), the possible reason for its formation is, upon UV irradiation, the organics in the POME would have decompose into smaller intermediate species and CH_4.

In addition, the total gas produced for all set of experiments were further calculated and tabulated in Table 3. Based on Table 3, photoreaction with 1.0 g/L TiO_2 produced the highest amount of gas products (CO_2 + CH_4), followed by 1.5 g/L 2.0 g/L, 0.7 g/L, 0.5 g/L and 0.1 g/L, consistent with the COD degradation results (cf. Figure 4a). Moreover, photoreaction over 1.0 g/L of TiO_2 yielded the most CO_2 (38913 μmol)

due to the highest degradation rate of organics. In terms of CH_4, the production of photoreaction with 0.5 g/L TiO_2 (361 μmol) was slightly higher compared to others under similar experimental conditions. On the other hand, the purity of CH_4 in gas products showed a contradicting trend with the increasing TiO_2 loading. Lower TiO_2 loadings (0.1 and 0.5 g/L; 1.7% and 1.6%) produced gas product with higher composition of CH_4 compared to the higher TiO_2 loadings. These could be reasonably deduced as lower TiO_2 loadings would degrade lesser organics, and eventually lower CO_2 formation rate; hence higher CH_4 composition in the gas product. For TiO_2 loadings higher than 0.7 g/L, the CH_4 composition in gas products was almost similar, ranging from 0.9 to 1.1%.

3.2.4 Mechanism Proposal

Based on the results obtained from both POME degradation and gaseous product formations, the mechanisms of POME decomposition during photocatalysis is proposed in Figure 8.

In the first step, $OH^{\bullet}$ radicals will be generated through (M1) to (M6). Then, these $OH^{\bullet}$ free radicals will directly attack the organics (denoted by $C_aH_bO_c$ in M7) in POME sample and degraded them into intermediate species, CH_4, H_2O and CO_2.

$$OH^{\bullet}_{,\,ads} + C_aH_bO_c \rightarrow \text{Intermediates} + CH_4 + H_2O + CO_2 \qquad \text{(M7)}$$

The oxygen-rich environment in the system inducing high oxidation possibility and eventually the organics have higher tendency to be degraded into CO_2 and H_2O compared to CH_4. Thus, the CH_4 composition should be comparatively low as proven experimentally from the current work.

3.2.5 Recyclability and Longevity Study

The stability of TiO_2 was studied from the view-point of practical application. A successful recyclable photocatalyst is very important for photo-degradation process of

wastewater. Based on previous findings, the best conditions for POME degradation is 70 ml/min of O_2 flowrate and 1.0 g/L of TiO_2. The recyclability of TiO_2 was demonstrated for three consecutive runs. Recovery of TiO_2 in between the runs was achieved by filtering process. Results obtained are presented in Figure 9. For the 1st-cycle, more than 51.0% degradation were achieved after 240 min of UV irradiation while for 2nd and 3rd cycles, the degradation reduced slightly to 48.0% and 49.0%, respectively. No significant deactivation of TiO_2 was observed, which confirmed the stability of the recyclability of TiO_2 in POME degradation.

Figure 10 shows the FTIR results for both fresh and used TiO_2 photocatalysts. OH and Ti-O bonds were detected at wavenumber of 3400 and 1650 cm^{-1}, respectively, for both fresh and recycled TiO_2. Apparently, no other functional groups were detected on the surface of used TiO_2. Besides, this also confirmed the results of adsorption study discussed earlier in Section 3.2.2, where adsorption of organic species on the TiO_2 surface was practically negligible. Significantly, this FTIR result also confirmed on the mechanisms proposed in Section 3.2.4 in which the $OH^{\bullet}$ formed will directly attack the organics without the need to adsorb on the photcatalyst's surface during the POME degradation process. Recently, Dong and coworkers[40] in their review paper have also confirmed the absence of organic compounds adsorption on the TiO_2 surface due to the poor affinity towards organic pollutants.

Finally, longevity test of 20 h was conducted. The comparisons of POME sample before and after photoreaction is presented in Figure 11a. Based on Figure 11a, POME sample was fully decolorized after 20 h of UV irradiation. As shown in Figure 11b, high degradation rate was observed during the first 2 h of the reaction. Thereafter, the exhaustion of the organics in the POME progressively slowed down the reaction.

As can be observed, after 20 h of photocatalytic reaction, about 78% of COD reduction were achieved, with 37 ppm as the final COD level of POME (initial = 168 ppm), which is safe for discharged. For gaseous product formations, once again, only the CO_2 and CH_4 were detected, with the total cumulative amounts of 77150 μmol and 1070 μmol, respectively, after 20 h of UV irradiation.

4. Conclusions

Based on the results obtained, the best TiO_2 loading for POME degradation was 1.0 g/L whereby 52.0% of organic removal was achieved after 240 min of UV irradiation. Significantly, CO_2 was the major gaseous component and the photoreaction with 1.0 g/L of TiO_2 released the highest amount of CO_2 (38913 μmol), whilst photoreaction with 0.5 g/L TiO_2 produced the highest amount of CH_4 (361 μmol). Our results also demonstrated that the $OH^{\bullet}$ radicals' generation was primarily from O_2 and not from H_2O that was readily present in the POME. Moreover, we proposed herein reaction pathways that involved firstly the $OH^{\bullet}$ radicals generation, followed by direct attack on the organics into smaller organic intermediates, CH_4 and also CO_2. In addition, recyclability and longevity studies were also conducted. Based on the recyclability study, no significant deactivation of TiO_2 was observed after three consecutive POME degradation runs. The degradation achieved were 51.0%, 48.0% and 49.0%, respectively. FTIR analysis of the post-reaction TiO_2 suggested an absence of organics adsorption on the TiO_2 surface. Therefore, we infer that instead of organic compounds adsorbed onto the TiO_2 surface, the organic compounds were directly attacked by the $OH^{\bullet}$ radicals and decomposed into gaseous products. Moreover, after 20 hours of UV irradiation, 78.0% of POME degradation were achieved and the COD level of POME dropped from 168 ppm to 37 ppm, which was lower than the permitted discharge limits (50 ppm). In lieu of the interesting results

that were obtained, our future work will include the optimization of the experimental conditions via the use of chemometrics[41, 42] or other similar softwares to reflect the multivariate behaviour of the system.

Acknowledgements

Authors feel grateful to the Ministry of Education Malaysia for the Exploratory Research Grant Scheme (ERGS) RDU120613 and also the Ministry of Science, Technology and Innovation Malaysia for Sciencefund scheme (RDU130501).

References

[1] T. Mielke, presented at Global supply, demand and price outlook for palm and lauric oils. In: 2nd palm oil Internet seminar, 22–29 July 2013.

[2] S. Yacob, M. A. Hassan, Y. Shirai, M. Wakisaka, & S. Subash, *Sci. Total. Environ*, 2006, **366**, 187-196.

[3] A. L. Ahmad, S. Sumathi, & B. H. Hameed, *Chem. Eng. J.*, 2005, **108**, 179–185.

[4] C. C. Ho, Y. K. Tan, & C. W. Wang, *Agric. Wastes*, 1984, **11**, 61–71

[5] K. Sundram, R. Sambanthamurthi, & Y. A. Tan, *J. Clin. Nutr.* ,2003, 355–362.

[6] S. J. Santosa, *CLEAN – Soil Air Water,* 2008, **36**, 453–65.

[7] A. A. L. Zinatizadeh, A. R. Mohamed, A. Z. Abdullah, M. D. Mashitah, I. M. Hasnain, & G. D. Najafpour, *Water Res.*, 2006, **17**, 3193–3208.

[8] T. Y. Wu, A. W. Mohammad, J. Md. Jahim, & N. Anuar, *Biochem. Eng. J.* , 2007, **3**, 309–317.

[9] W. Choorit & P. Wisarnwan, *Electron. J. Biotech.* ,2007, **3**, 3193–3208.

[10] American Palm Oil Council, http://www.americanpalmoil.com/ (accessed March 2015.

[11] L. K. Wang, J. Tay, S.T.L. Tay, & Y. Hung, *Springer Sci. Bus. Media* ,2010, 653–654.

[12] Malaysia Palm Oil Board, http://www.mpob.gov.my/ (accessed March 2015)

[13] Y. J. Chan, M. F. Chong, & C. L. Law, *J. Environ. Manage*, 2010, **91**, 1738-1746.

[14] A. L. Ahmad, S. Ismail, & S. Bhatia, *Desalination*, 2003,**157**, 87-95.

[15] Y. Zhang, L. Yan, X. Qiao, L. Chi, X. Niu, Z. Mei, & Z. Zhang, *J. Environ Sci.*, 2008, **20**, 558-564.

[16] F. Shahrezaei, Y. Mansouri, A. A. L. Zinatizadeh, & A. Akhbari, *International Journal of Photoenergy,* 2012, doi:10.1155/2012/430638.

[17] V. J.P. Vilar', L. X. Pinho, A. M. A. Pintor, & R. A. R. Boaventura, *Sol. Energ.,* 2011, **85**, 1927-1934.

[18] C. S. Lima, K. A. Batista, A. G. Rodríguez, J. R. Souza, & K. F. Fernandes, *Sol Energ.* 2015, **114**, 105-113.

[19] A. Hameed & M. A. Gondal, *J. Molecular Catalysis A* , 2005, **233**, 35.

[20] P. Panagiotopoulou, E. E. Karamerou, & D. I. Kondarides, *Catal. Today*, 2013, **209**, 91-98.

[21] M. P. Languer, F. R. Scheffer, A. F. Fell, D. L. Baptista, P. Migowski, G. J. Machado, D. P. De Moraes, J. Dupont, S. R. Teixeira, & D. E. Weibel, *Int. J. Hydr. Energ.* 2013, **38**, 14440-14450.

[22] K. H. Ng, M. R. Deraman, C. H Ang, S. K. Chong, Z. Y. Kong, M. R. Khan, & C. K. Cheng, *Bullentin of Chemical Reaction Engineering & Catalysis,* 2014, **9**, 121-127.

[23] C. K. Cheng, M. R. Deraman, & M. R. Khan, *Journal of Environmental Chemical Engineering*,DOI: 10.1016/j.jece.2014.10.016.

[24] R. Amadelli, A. Molinari, I. Vitali, L. Samiolo, G. M. Mura, & A. Maldotti, *Catal. Today,* 2005, **101**, 397-405.

[25] Fujishima, T. N. Rao, and D. A. Tryk, *J.Photoch. Photobio. A.*, 2000, 1, 1-21.

[26] K. H. Wang, Y. H. Hsieh, L. J. Chen, *J. Hazard. Mater.* 1998, **59**, 251–260.

[27] N. Barka, I. Bakas,S. Qourzal, A. Assabbane, & Y. Ait-Ichou, *Orient. J. Chem.*, 2013, doi : http://dx.doi.org/10.13005/ojc/290328.

[28] M. Choquette-Labbé, W. Shewa, J. Lalman, & S. Shanmugam, *Water*, 2014, http://dx.doi.org/10.3390/w6061785.

[29] X-Ray Diffraction, E. Warren, *Courier Dover Publications*, 1969.

[30] S. Valencia, J. M. Marin, and G. Restrepo. *The Open Materials Science Journal,* 2010, **4**, 9-14.

[31] M. A. Lazar & W. A. Daoud, *RSC Adv.*, 2013,**3**, 4130-4140

[32] A. Mills, R. H. Davies, D. Worsley, *Chemical Society Reviews*, 1993, **22**(6), 417-25.

[33] B. Neppolian, H. C. Choi, S. Sakthivel, B. Arabindoo, & V. Murugesan, *Chemosphere*, 2002, **46**,1173–1181.

[34] H. Goto, Y. Hanada, T. Ohno, M. Matsumura, *J. Catal*., 2004, **225,** 223-229.

[35] T. Hirakawa, C. Koga, N. Negishi, K. Takeuchi, & S. Matsuzawa, *Appl. Catal., B: Environmental*, 2009, **87**, 46-55.

[36] H. S. Fogler, Elements of Chemical Reaction Engineering, Prentice Hall, US, 4th edn., 2005.

[37] D. C. Montgomery, Design and Analysis of Experiment, John Wiley & Sons, New York, 4th edn., 1997.

[38] S. Manickam, N. Z. Abidin, S. Parthasarathy, I. Aizorqi, E. H. Ng, T. J. Tiong, R. L. Games, & A. Ali, *Ultrason. Sonochem*., 2014, **21**, 1519-1526.

[39] J. Speight, Lange's Handbook of Chemistry, McGraw-Hill, New York, 16th edn, 2004.

[40] H. Dong, G. Zeng, L. Tang, C. Fan, C. Zhang, X. He, & Y. He, *Water Res.*, 2015, **79**, 128-146.

[41] F. Bella, M. Imperiyka, & A. Ahmad, *J. Photochem. Photobiol., A: Chemistry*, 2014, **289**, 73-80.

[42] J. Song, J. Xie, C. Li, J. Lu, Q. Meng, Z. Yang, R. J. Lee, D. Wang, & L. Teng, *Int. J. Pharm.,* 2014, **472** (1-2), 296-303.

List of Figures

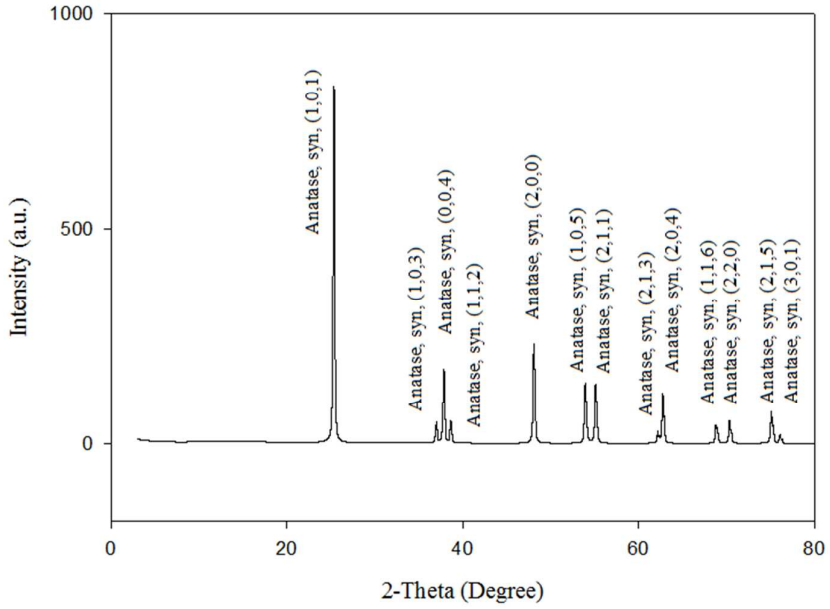

(a)

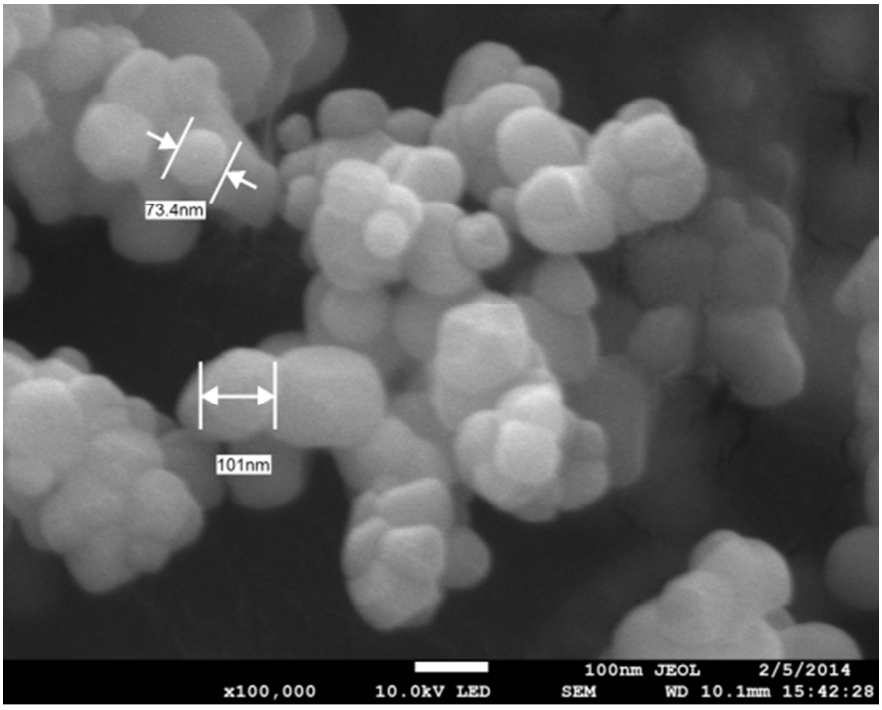

(b)

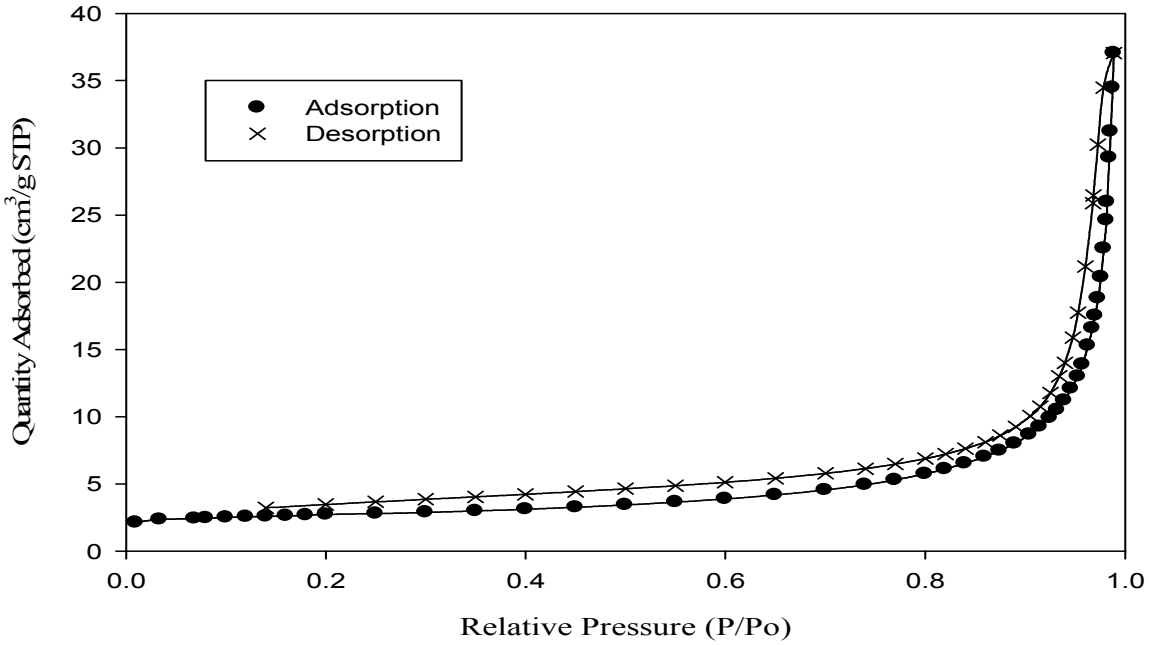

(c)

Figure 1 (a) XRD diffractogram of TiO_2. (b) FESEM images of TiO_2. (c) Isotherm of TiO_2

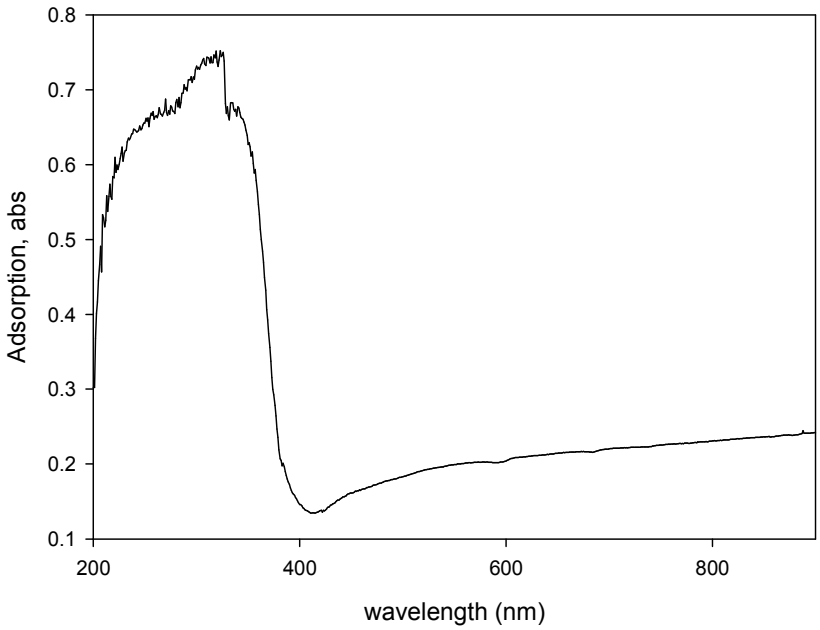

(a)

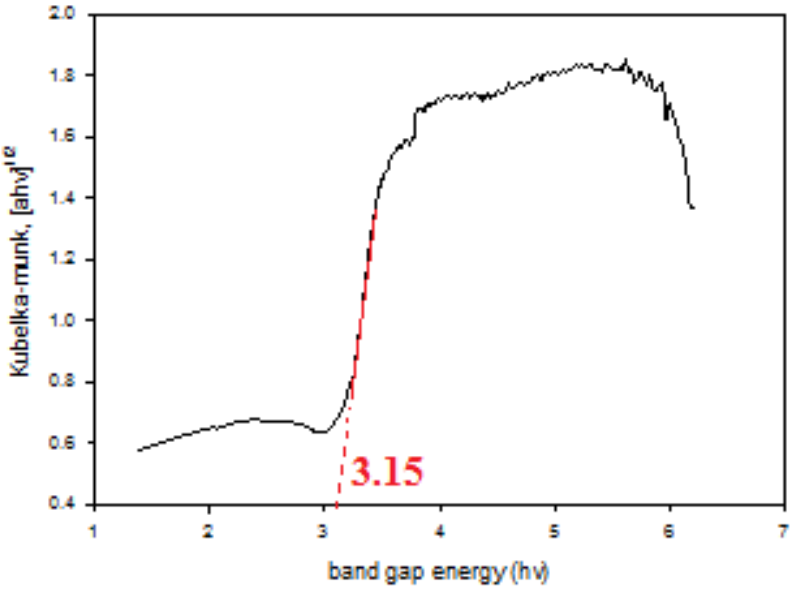

(b)

Figure 2 (a) Diffuse reflectance UV-Vis spectra of the photo-catalysts. (b) Plot of Kubelka-Munk function versus energy of light for TiO_2.

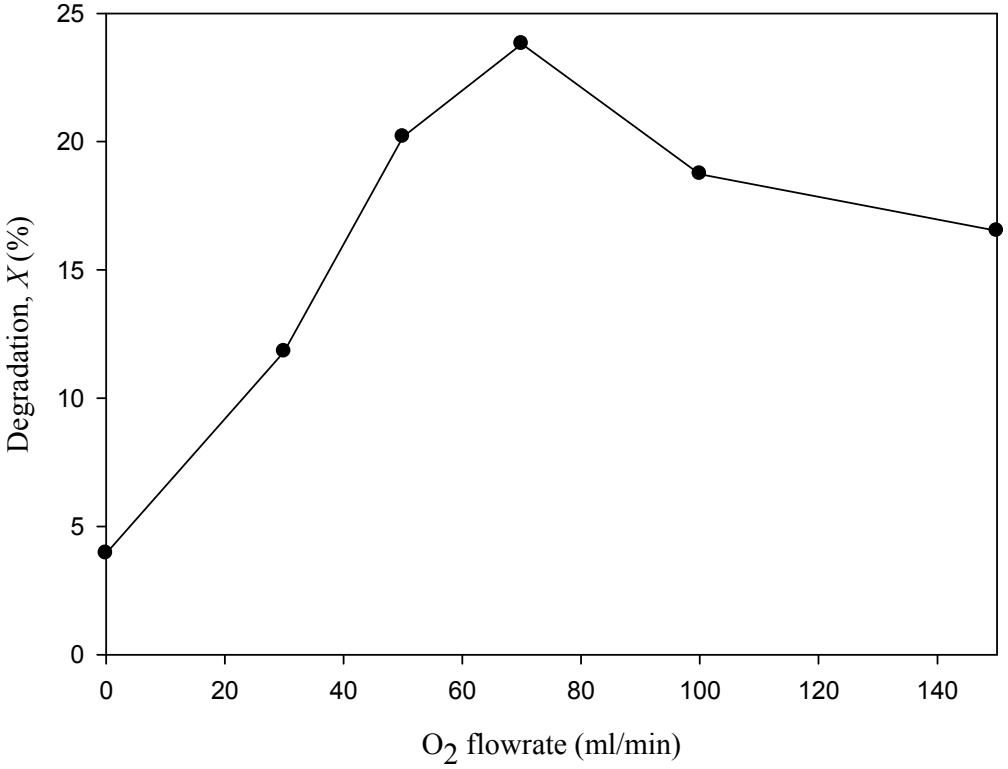

Figure 3 Degradation of POME after 240 min of UV irradiation with different O_2 flowrates. Reaction condition: 0.5 g/L TiO_2 at room temperature.

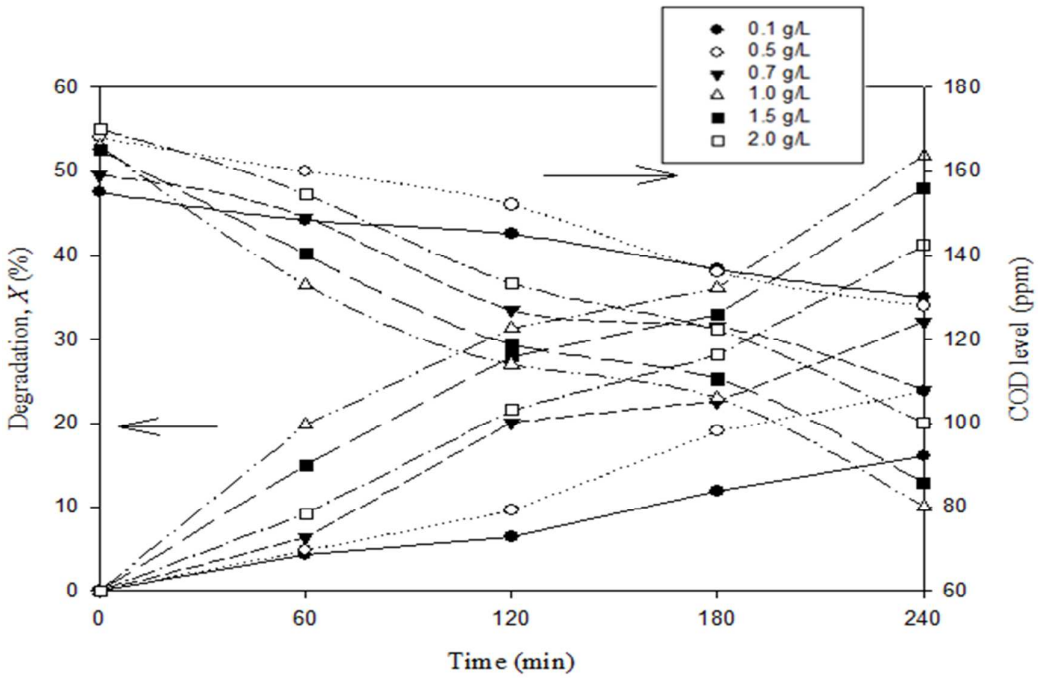

(a)

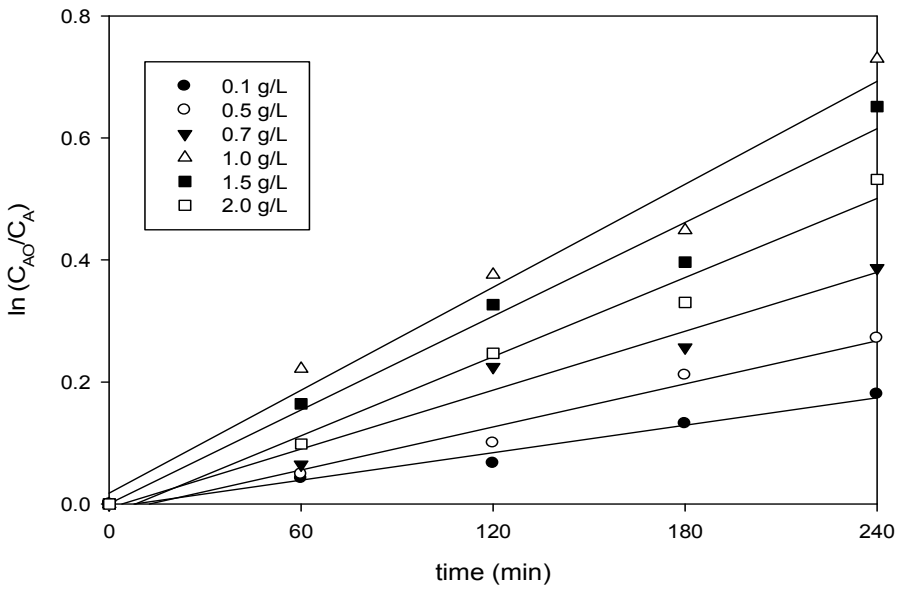

(b)

Figure 4 (a)Transient COD level (ppm) and degradation (%) profiles for photoreactions at different TiO_2 loadings. (b) Illustration showing good adherence to 1st order kinetics modelling.

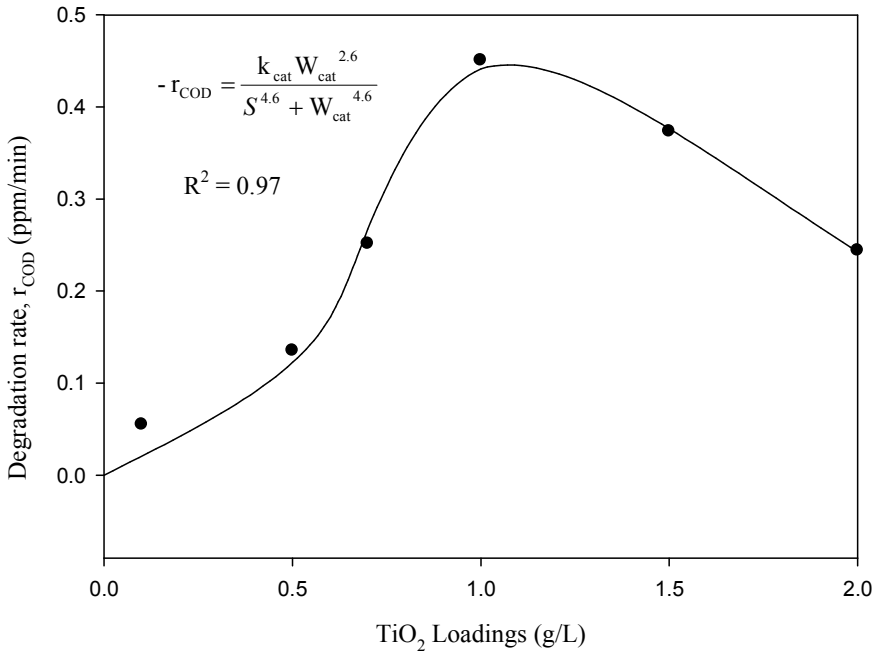

Figure 5 Influence of TiO_2 loadings on the degradation rate.

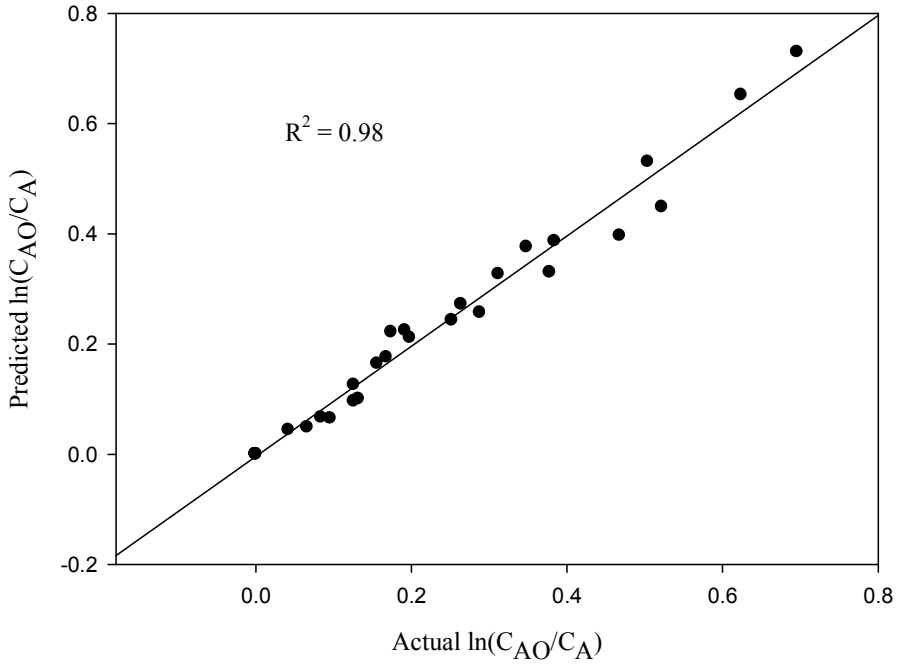

Figure 6 Comparison between predicted and actual $\ln(C_{AO}/C_A)$ values.

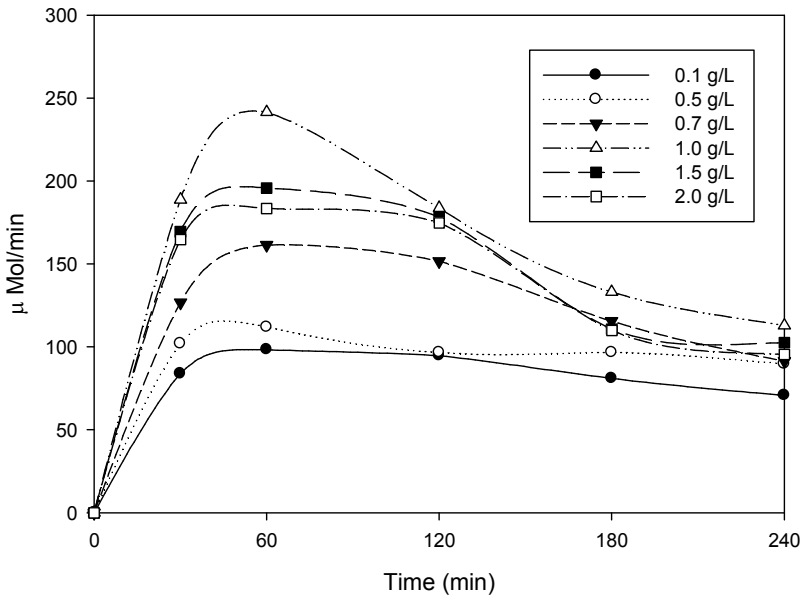

(a)

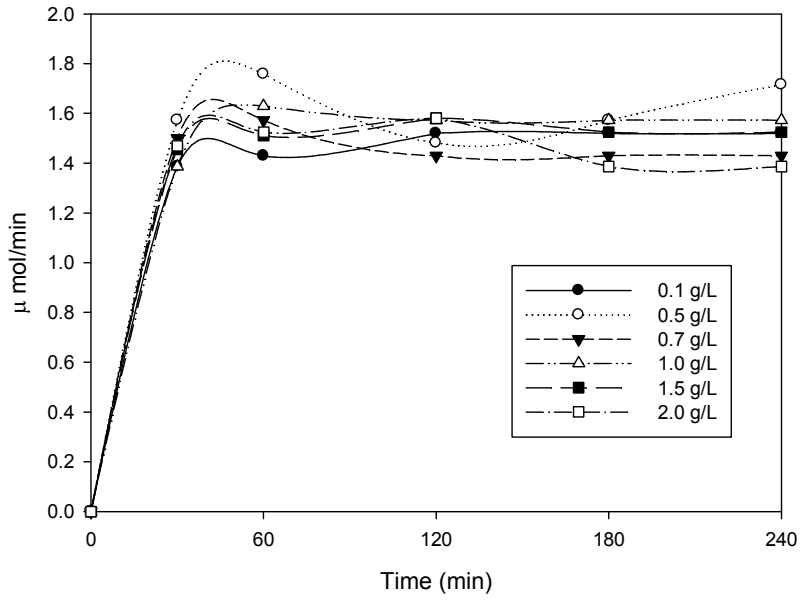

(b)

Figure 7 Gas products collected along the photoreaction with O_2 flowrate of 70 ml/min and temperature maintained at room temperature. (a) CO_2 (b) CH_4

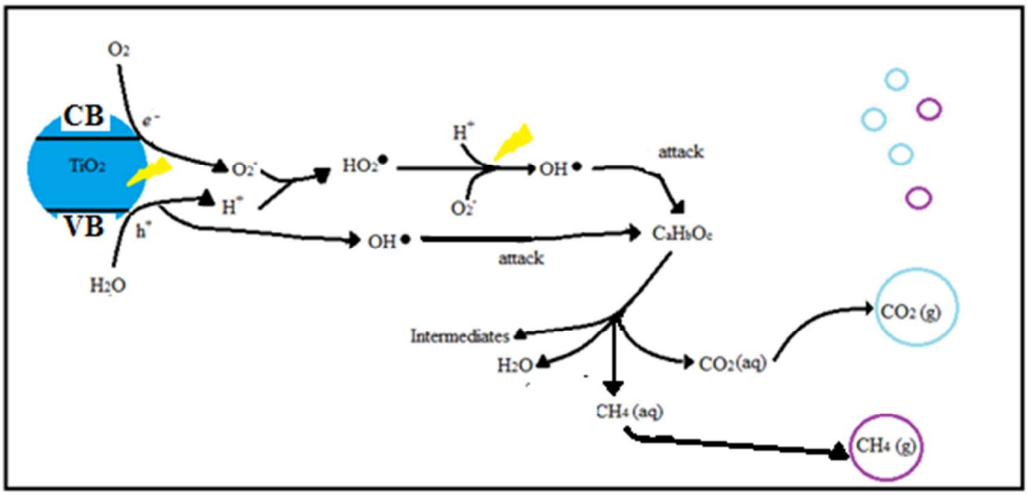

Figure 8 The schematic diagram of POME photocatalytic degradation mechanism.

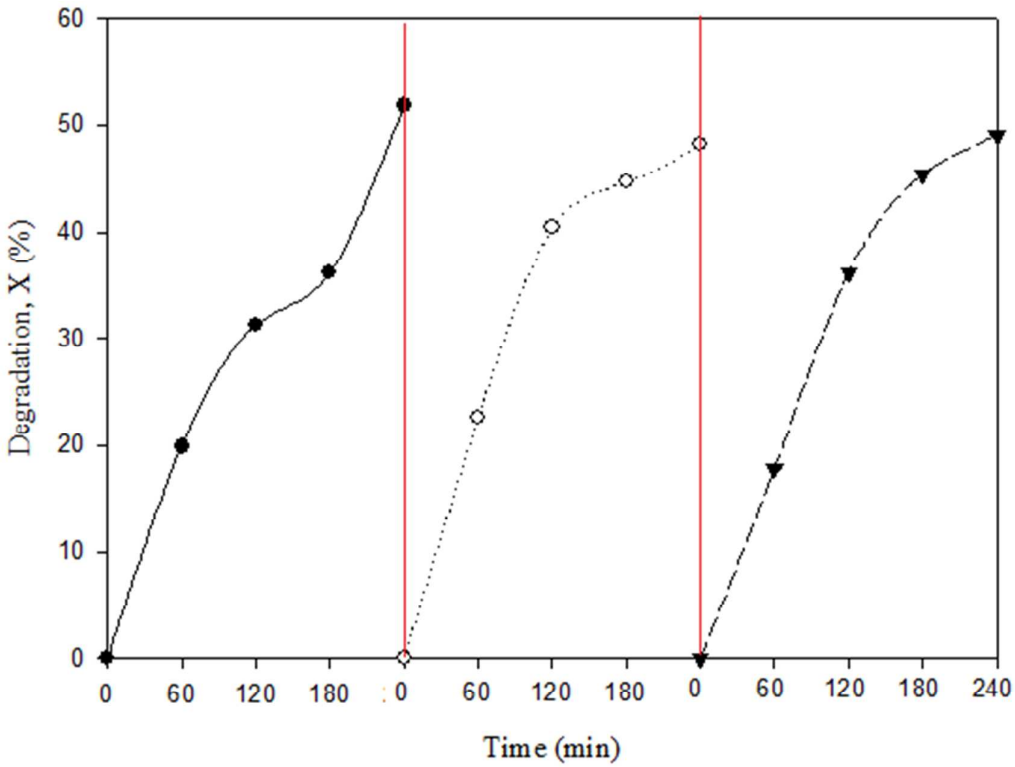

Figure 9 Degradation of POME with recycled TiO_2 over three consecutive runs.

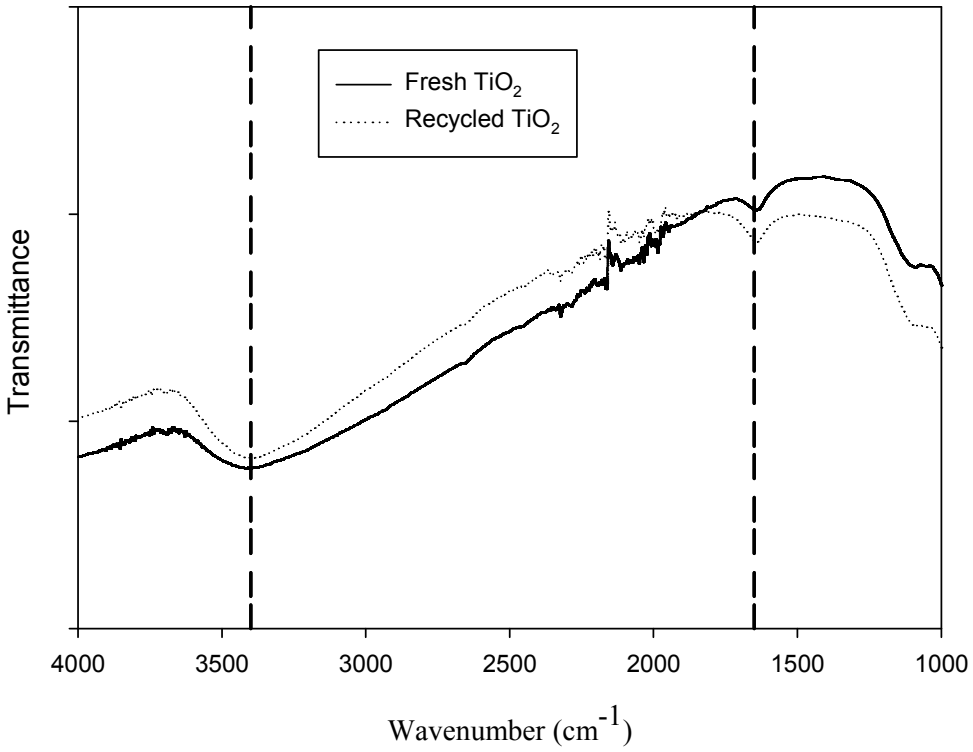

Figure 10 FTIR results of fresh and used TiO_2 photocatalysts.

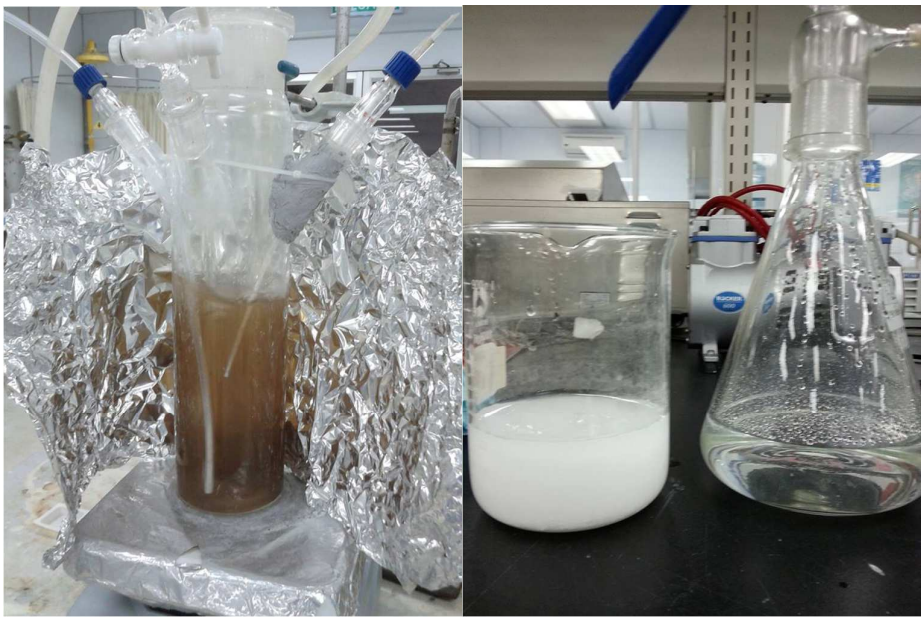

(a)

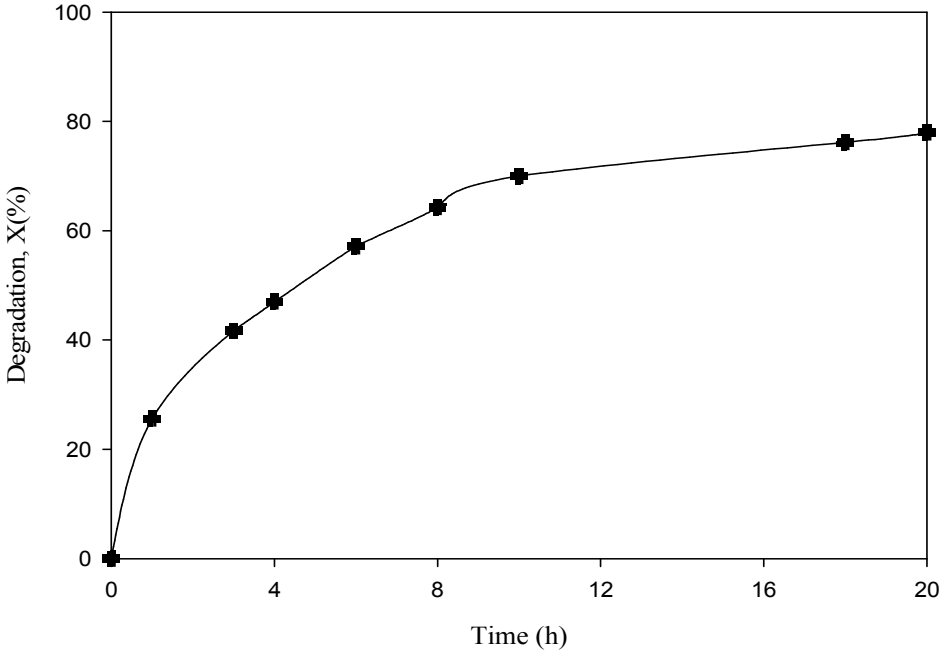

(b)

Figure 11 (a)POME sample at t = 0 min (left) and t = 20 h (right). (b) Degradation of POME for longevity study.

List of Table

Table 1 Comparisons of dischargable wastewater standard with POME samples.

Parameter	*Standard A*	POME-1	POME-2
COD	50	170	240
BOD	20	80	126
pH	6.0-9.0	7.5	7.5

*all the units are in ppm.

Table 2 *k*-values obtained from the photoreactions on POME with different TiO_2 loadings.

TiO_2 loading (g/L)	(k) $\times 10^3$ $(min)^{-1}$	R^2
0.1	0.70	0.98
0.5	1.10	0.97
0.7	1.60	0.97
1.0	2.90	0.97
1.5	2.60	0.98
2.0	2.10	0.98

Table 3 Total gas products collected from photoreactions.

TiO_2 loadings (g/L)	Gas accumulated over 240 min of photoreaction (μmol)		CH_4 composition (%)
	CO_2	CH_4	
0.1	19599	334	1.7
0.5	22384	361	1.6
0.7	29823	330	1.1
1.0	38913	351	0.9
1.5	34291	344	1.0
2.0	33124	332	1.0